AGU PUBLICATIONS

Paleoceanography

RESEARCH ARTICLE
10.1002/2015PA002780

Impact of global SST gradients on the Mediterranean runoff changes across the Plio-Pleistocene transition

Florence Colleoni[1], Annalisa Cherchi[1,2], Simona Masina[1,2], and Christopher M. Brierley[3]

[1]Centro Euro-Mediterraneo sui Cambiamenti Climatici, Bologna, Italy, [2]Instituto Nazionale di Geofisica e Vulcanologia, Bologna, Italy, [3]Department of Geography, University College London, London, UK

Key Points:
- Annual mean Pliocene Mediterranean runoff is 40% larger than today
- Global SST cooling increases water deficit due to lower precipitation and runoff
- Changes in Hadley circulation could increase water supply in northwest Africa

Correspondence to:
F. Colleoni,
florence.colleoni@cmcc.it

Citation:
Colleoni, F., A. Cherchi, S. Masina, and C. M. Brierley (2015), Impact of global SST gradients on the Mediterranean runoff changes across the Plio-Pleistocene transition, *Paleoceanography*, *30*, doi:10.1002/2015PA002780.

Received 15 JAN 2015
Accepted 15 MAY 2015
Accepted article online 20 MAY 2015

Abstract This work explores the impact of the development of global meridional and zonal sea surface temperature (SST) gradients on the Mediterranean runoff variability during the Plio-Pleistocene transition, about 3 Ma. Results show that total annual mean Pliocene Mediterranean runoff is about 40% larger than during the preindustrial period due to more increased extratropical specific humidity. As a consequence of a weakened and extended Hadley cell, the Pliocene northwest Africa hydrological network produces a discharge 30 times larger than today. Our results support the conclusion that during the Pliocene, the Mediterranean water deficit was reduced relative to today due to a larger river discharge. By means of a stand-alone atmospheric general circulation model, we simulate the separate impact of extratropical and equatorial SST cooling on the Mediterranean runoff. While cooling the equatorial SST does not imply significant changes to the Pliocene Mediterranean hydrological budget, the extratropical SST cooling increases the water deficit due to a decrease in precipitation and runoff. Consequently, river discharge from this area reduces to preindustrial levels. The main teleconnections acting upon the Mediterranean area today, i.e., the North Atlantic Oscillation during winter and the "monsoon-desert" mechanism during summer already have a large influence on the climate of our Pliocene simulations. Finally, our results also suggest that in a climate state significantly warmer than today, changes of the Hadley circulation could potentially lead to increased water resources in northwest Africa.

1. Introduction

Over the last 5 million years (Myrs), the Earth's climate experienced a gradual cooling [*Lisiecki and Raymo*, 2005], which resulted in the growth of continental ice sheets over the Northern Hemisphere high latitudes from about 3.3 Ma [*Jansen et al.*, 2000; *Haug et al.*, 2005]. The analysis of marine records from the Mediterranean has revealed that this region was impacted by the major global climate changes that occurred over the last 5 Myrs [*Colleoni et al.*, 2012; *Herbert et al.*, 2015]. In particular, the Mediterranean planktonic record [*Wang et al.*, 2010; *Lourens*, 2004] and the recent sea surface temperature (SST) reconstruction [*Herbert et al.*, 2015] show that Mediterranean climate variability was mainly driven by precession, which has been related to the influence of the African monsoon [*Rossignol-Strick*, 1985] until the Plio-Pleistocene transition. Evidence that the Mediterranean was influenced by the onset of Northern Hemisphere glaciations is supported by different types of terrestrial and marine records. The incursions of cold foraminifera species recorded in the Mediterranean marine sediments suggest that the cold Atlantic surface waters started to penetrate into the Mediterranean around 2.5 Ma [*Lourens et al.*, 1992]. This is further supported by a recent Mediterranean sea surface temperature (SST) record [*Herbert et al.*, 2015] indicating that the first noticeable cooling of the Mediterranean Sea occurred near 2.5 Ma (Figure 1). Moreover, *Bertini* [2010], *Salzmann et al.* [2008], and *Leroy and Dupont* [1994] show that the Mediterranean vegetation changed from temperate mixed forest, indicative of a warm and wet climate, to temperate deciduous forest, indicative of a cold and dry climate, after about the Plio-Pleistocene transition (Figure 1). In addition, analysis of the Mediterranean planktonic stack [*Colleoni et al.*, 2012] shows that after 3 Ma, the amplitude of the δ^{18}O oscillations increased gradually (Figure 1), suggesting a change in hydrological conditions.

Although cooling was recorded on a global scale [*Fedorov et al.*, 2013], marine records from different areas show that it happened diachronously in the high latitudes and in the tropics (Figure 1). According to open-ocean SST proxies, the Northern high latitudes started to cool significantly from 3.3 Ma [*Lawrence et al.*, 2010] almost concomitantly with the Southern high latitudes [*Martinez-Garcia et al.*, 2010; *McKay et al.*, 2012], leading to a stronger interhemispheric meridional SST gradient. Though the structure and the evolution of

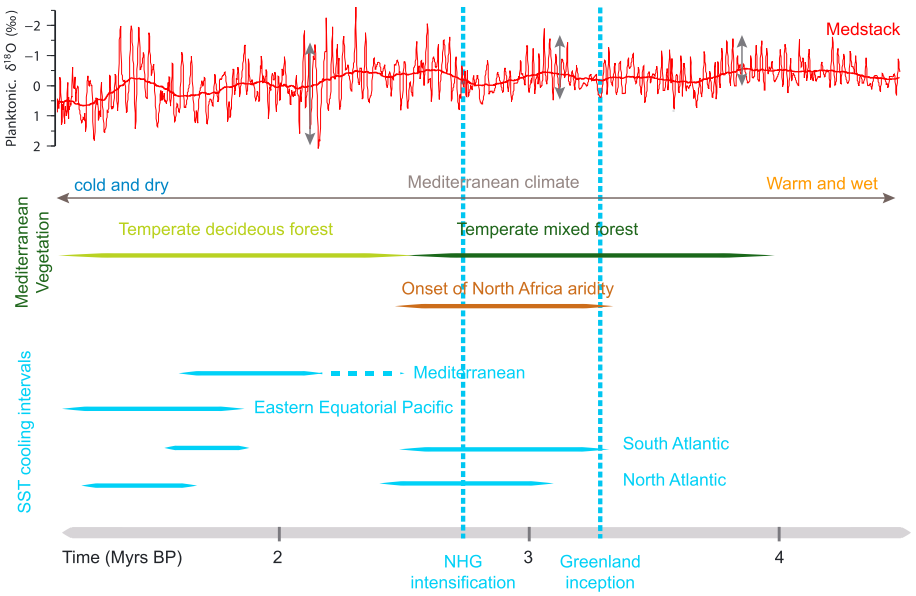

Figure 1. Comparison between the various proxies dealing with the Mediterranean climate and discussed in the present work. From top to bottom: Mediterranean planktonic δ^{18}O record [*Wang et al.*, 2010; *Lourens*, 2004]; Northern Mediterranean vegetation changes after [*Salzmann et al.*, 2008; *Leroy and Dupont*, 1994]; sea surface temperature (SST) cooling observed in the Mediterranean [*Herbert et al.*, 2015], in the North Atlantic [*Lawrence et al.*, 2010], in the South Atlantic [*Martinez-Garcia et al.*, 2010; *McKay et al.*, 2012], and in the Eastern Equatorial Pacific [*Martinez-Garcia et al.*, 2010]. In addition, Greenland ice sheet inception [*Jansen et al.*, 2000] and the intensification of Northern Hemisphere glaciation [*Haug et al.*, 2005] are indicated.

the zonal equatorial SST gradient after the Plio-Pleistocene transition is still debated [*O'Brien et al.*, 2014], some marine temperature proxies suggest that the Eastern Equatorial Pacific and Atlantic cold tongues started to expand substantially toward 1.8 Ma [*Wara et al.*, 2005; *Ravelo et al.*, 2004; *Martinez-Garcia et al.*, 2010; *Lawrence et al.*, 2010; *Pagani et al.*, 2010], strengthening the zonal SST gradient in both Pacific and Atlantic basins [*Etourneau et al.*, 2010]. This later phase of cooling is also observed in the Mediterranean SST and planktonic δ^{18}O records [*Colleoni et al.*, 2012; *Herbert et al.*, 2015]. The impact of the meridional and zonal SST gradients on the global climate during the end of the Pliocene have been previously investigated. During the warm Pliocene, geological evidence suggests that both meridional and zonal SST gradients were weak [*Wara et al.*, 2005; *Ravelo et al.*, 2004; *Fedorov et al.*, 2013] and that the Arctic sea ice cover was mostly seasonal [*Polyak et al.*, 2010, 2013]. The causes and the consequences of such a surface ocean structure are still under investigation and highly debated [e.g., *Fedorov et al.*, 2006; *Barreiro et al.*, 2006; *Brierley et al.*, 2009; *O'Brien et al.*, 2014]. Nevertheless, all those studies report higher global temperatures, potentially accompanied by higher global precipitation rates, a weakening of the Hadley circulation and a collapse of the Walker circulations in response to the Pliocene surface ocean conditions. In a more recent study, *Brierley and Fedorov* [2010] investigate the impact of meridional and zonal SST gradients on the onset of Northern Hemisphere glaciations and show that the boreal lands are able to freeze when the meridional SST gradient strengthens, i.e., when SST start to cool in the high latitudes. Because the current Mediterranean climate is partly influenced by the descending branch of the Hadley cell [*Raicich et al.*, 2003], changes in the global meridional and zonal SST gradient during the Plio-Pleistocene transition potentially have a large influence on the Mediterranean hydrological cycle.

So far, no modeling study has specifically investigated the changes in precipitation and river discharge in the Mediterranean during this period. In this framework, the present study aims at investigating the influence of the Plio-Pleistocene climate cooling through the development of the global meridional and zonal SST gradients on the Mediterranean runoff and precipitation. The current Mediterranean hydrological cycle is unbalanced. The mean annual precipitation, about 400 mm/yr and the mean annual runoff, about 100 mm/yr, do not compensate for the large evaporation rates occurring over the Mediterranean Sea (≈1000 mm/yr). This causes a water deficit of about 500 mm/yr [*Mariotti et al.*, 2002]. In its past climate history, the Mediterranean experienced dramatic changes of its hydrology, i.e., a large part of the basin evaporated (but maybe not totally [e.g., *Roveri et al.*, 2014]) mainly due to the closure of the Mediterranean-Atlantic seaway during the

Messinian, about 5.96 Ma to 5.33 Ma [e.g., *Krijgsman et al.*, 1999]. At shorter time scales, the precession-paced depositions of enriched carbon layers, namely, "sapropels," mostly resulting from larger input in freshwater in the Mediterranean, testify to frequently altered hydrological conditions in this area over at least the last 5 Myrs [e.g., *Rossignol-Strick et al.*, 1982; *Lourens et al.*, 1992]. The issue of water resources is becoming a critical aspect of the mitigation and adaptation strategies to the ongoing climate changes and the Mediterranean region has been indicated as one of the most responsive area to climate change, a so called "hot spot" [*Giorgi*, 2006]. Studying the Mediterranean past warm climate history allows us to better understand the evolution of the hydrological cycle under similar or warmer climate conditions. From this perspective, the Pliocene period is ideal to investigate this issue since the CO_2 atmospheric concentration was found similar to present-day levels [*Pagani et al.*, 2010] and global land ice volume was substantially smaller than today by ≈25 m of sea level equivalent [e.g., *Raymo et al.*, 2011]. Moreover, the Mediterranean configuration was similar to today for the first time.

Here we use an atmosphere-land-sea-ice model (CAM4 coupled to CLM4 and CICE4) forced by present-day, preindustrial and Mid-Pliocene SST reconstructions following *Brierley and Fedorov* [2010]. The approach of the present study is idealized and does not aim at reproducing realistic climate conditions through the Plio-Pleistocene transition. In subsequent sensitivity simulation, we prescribe modern extratropical SST in the Pliocene experiment in agreement with the high-latitude SST cooling detected in the sediment records (Figure 1) and use tropical Pliocene SST. For further sensitivity experiments, we prescribe modern tropical SST in the Pliocene experiment and use extratropical Pliocene SST to test the separate impact of the development of the zonal equatorial SST gradient on the Mediterranean climate. Similar to previous studies using a stand-alone atmospheric model, e.g., *Haywood et al.* [2010, 2011], all other Pliocene boundary conditions, i.e., vegetation and topography are prescribed from PRISM3D project [*Dowsett et al.*, 2009]. The aim of these experiments are (i) to quantify the Pliocene Mediterranean runoff relative to modern one, (ii) to quantify the changes in the Mediterranean hydrological cycle due to the strengthening of the meridional and zonal SST gradients, and (iii) understand what are the changes in synoptic and regional circulation leading to those runoff and precipitation variations. The manuscript reads as follows: in section 2, we describe the model and the design of the experiments. We analyze the outcomes of the simulations in section 3, and we finally draw our conclusions in section 4.

2. Methods

2.1. Climate Model

Our simulations have been carried out using version 4 of the Community Atmosphere Model (CAM 4) coupled to the Community Land Model (CLM 4) and to the Community Sea-Ice Model (CICE 4) [*Neale et al.*, 2013]. SSTs are prescribed (see section 2.2 below) and SSTs colder than −1.8°C are treated as sea ice. The atmospheric component CAM 4 has 26 vertical levels, and we use the horizontal grid resolution of 0.9° × 1.25° shared with the land (CLM 4) and the sea ice component (CICE 4). Runoff is computed using a TOPMODEL-based model implemented within CLM 4 [*Niu et al.*, 2007]. The concept of this model relies on the calculation of the overland flow caused by saturation and infiltration excess in the soil. The river discharge is computed through the River Transport Model (RTM) implemented within CLM 4 [*Oleson et al.*, 2008]. The RTM uses a linear transport scheme at 0.5° resolution that approximates the path of the real global river network (based on a 1 km DEM map) to route the runoff computed by the land model to the rivers mouths. The vegetation is not interactive and the distribution of the different biomes is prescribed as boundary condition.

In CAM 4, a finite volume dynamical core (CAM4-FV) is implemented and provides substantial improvements compared to the spectral grid version [*Neale et al.*, 2013]. In particular, regional precipitation is improved in CAM 4. Specifically, the excessive Indian monsoon rainfall decreases compared to CAM 3 and the Northern Hemisphere western ocean rainfall deficit is reduced [*Neale et al.*, 2013]. River discharge has been validated for CLM3.5 in *Oleson et al.* [2008] by comparing the modeled values with observations at the main global river mouths. Performances were found to be generally high and although the Mediterranean region presented the lowest correlation between model and observations, it nevertheless reached a correlation of 0.85 [*Oleson et al.*, 2008]. In the present version of CLM 4, the runoff scheme and the RTM model have been improved and the global biases have been significantly reduced.

2.2. Sea Surface Temperature Forcing

The main idea in this study is to test the separate impact of stronger global meridional and zonal SST gradients relative to Pliocene SST conditions on the precipitation regime and river discharge in the Mediterranean

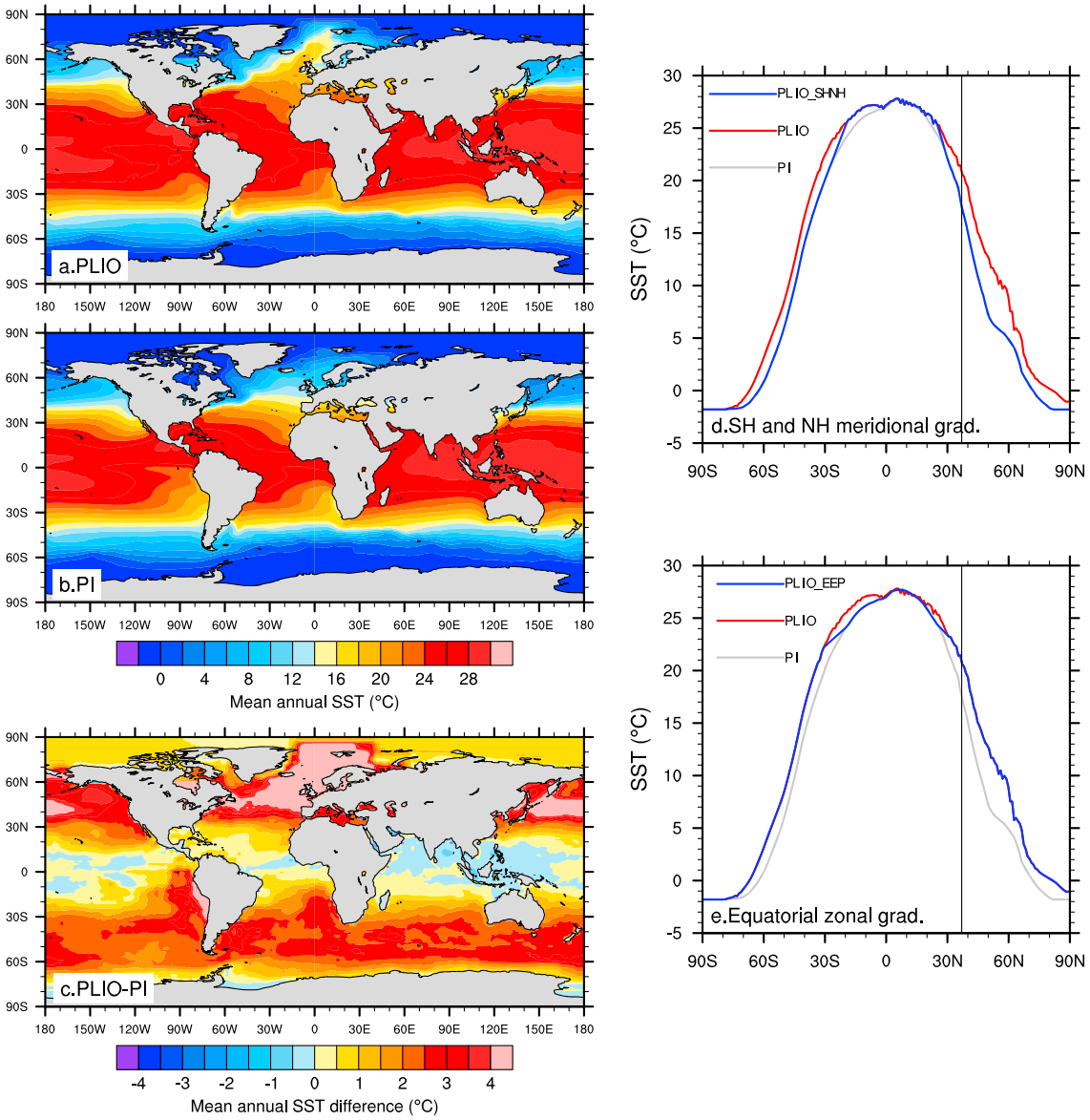

Figure 2. Boundary forcing for the numerical experiments (see Table 1): (a) Pliocene SST reconstruction from PRISM3 [*Dowsett et al.*, 2009]; (b) preindustrial Hadley Center SST reconstruction for PI control run; (c) difference between Pliocene and preindustrial SST (°C). Global zonal mean average of SST used to force the sensitivity experiments where meridional and zonal SST gradients are included: (d) profiles of PI (gray line), PLIO (red line) and PLIO_SHNH (blue line) where the tropics coincide with PLIO and the extratropics with PI; (e) profiles of PI (gray line), PLIO (red line) and PLIO_EEP (blue line) where the tropics coincide with PI and the extratropics with PLIO. Vertical black line localizes the mean latitude of the Mediterranean sector (37°N). For more details about the settings of the experiments, see Table 1.

region across the Plio-Pleistocene transition (≈3 Ma). The choice of considering the meridional and zonal SST gradients separately is motivated by geological proxies showing that the strengthening of the global meridional SST gradient at the end of the Pliocene and beginning of the Pleistocene preceded the expansion of the Pacific and Atlantic Equatorial cold tongues [*Lawrence et al.*, 2010; *Martinez-Garcia et al.*, 2010]. We follow the work of *Brierley and Fedorov* [2010] who tested the impact of idealized meridional and zonal SST gradients on the onset of the Northern Hemisphere glaciations during the Plio-Pleistocene transition, but here we use different boundary conditions. We use the Pliocene SST reconstruction from the PRISM3D project [*Dowsett et al.*, 2009] and the preindustrial SST reconstruction from the Hadley Center [*Rayner et al.*, 2003] as shown in Figure 2c. To isolate the impact of the zonal equatorial SST gradient, we combined preindustrial tropical SST (30°S–30°N) with extratropical SST from Pliocene PRISM3D reconstruction (Figure 2d). To investigate the impact of the global meridional SST gradient, we combined preindustrial SST for extratropical latitudes with

Table 1. Settings of Climate Simulations[a]

ID	Epoch	Ecc.	Perihelion (date)	Obl. (deg)	CO_2 (ppm)	SST	Spin-Up	Length (model-years)
CTR0k	1990 A.D.	0.0167	4 Jan	23.44	367	HadOIBl	-	100
PI	1850 A.D.	0.0167	4 Jan	23.44	284	HadISST	-	100
PLIO	3.092 Myr	0.0326	7 Feb	22.93	405	PRISM3	-	100
PLIO_EEP	3.092 Myr	″	″	″	″	SST_{EEP}	PLIO	50
PLIO_SHNH	3.092 Myr	″	″	″	″	SST_{SHNH}	PLIO	50

[a]ID, Experiment ID; Epoch, Epoch of orbital configuration; Ecc., Eccentricity; Perihelion, Perihelion Date; Obl., Obliquity; CO_2, CO_2 atmospheric Concentration; SST, Data set for SST reconstruction; Spin-up, simulation used to initialize the climate model; and Length, Length of the simulations. In total, six experiments have been carried out: a preindustrial control run (PI), a warm Pliocene control run (PLIO), and four Pliocene experiments, branched on the fiftieth year of the PLIO control run and accounting for different SST gradients as described in Figure 2. The preindustrial control run was forced using HadISST SST from *Rayner et al.* [2003], while the Pliocene control run was forced using PRISM3 reconstruction [*Dowsett et al.*, 2009]. The SST forcing used in the four Pliocene experiments differ from PRISM3 Pliocene reconstruction: PLIO_EEP has PI equatorial zonal SST gradient over 30°S–30°N and Pliocene SST elsewhere; PLIO_SHNH has Pliocene SST in the tropical band (30°S–30°N) and PI extratropical SST elsewhere (Figure 2). All the Pliocene experiments are forced with the same orbital parameters taken from *Dolan et al.* [2011], use Pliocene CO_2 atmospheric concentration from *Dolan et al.* [2011], and keep CH_4 and N_2O to their preindustrial values, respectively.

Pliocene tropical SST for latitudes 30°S–30°N (Figure 2e). The details of the experiments performed using these forcing are described in the next section.

2.3. Numerical Experiments

To explore the Mediterranean runoff variability, five sensitivity experiments have been carried out: one present-day control run (CTR0k) to validate the Mediterranean river discharge against observations, one preindustrial control run (PI) to compare with the Pliocene simulations, a Pliocene control run (PLIO), which serves as reference to stress the differences resulting from the SST forcing, and two Pliocene simulations (PLIO_EEP, PLIO_SHNH), each of them accounting for one of the SST forcing described in Figure 2.

As boundary conditions, present-day and preindustrial control runs use present-day topography, vegetation distribution, and SST observations and reconstructions from Hadley Center [*Rayner et al.*, 2003], respectively (Table 1). The Pliocene experiments use the reconstructed PRISM3D topography, vegetation distribution [following *Rosenbloom et al.*, 2013] and SST [*Sohl et al.*, 2009; *Dowsett et al.*, 2009]. The main differences between the Pliocene reconstructed topography and present-day one reside in the absence of West Antarctic ice sheet, a substantial reduction in Greenland ice sheet and Rocky mountains elevation (not shown). Pliocene SST reconstruction has extratropical temperatures from 2°C to 3°C warmer than preindustrial SST (Figure 2a to 2c). Both Eastern Equatorial Pacific and Atlantic Pliocene SST are warmer by 3°C, which reduces the zonal SST gradient compared to preindustrial SST reconstruction. Over the tropics, SSTs show no significant difference between preindustrial and Pliocene, which is in agreement with geological evidence [*Dowsett et al.*, 1996] although *O'Brien et al.* [2014] suggest that SST might have been different. Arctic sea ice cover is largely reduced in the Pliocene reconstruction compared to preindustrial. This leads to SST being warmer by about 10°C in the North Atlantic, in the Nordic Seas, and in the North Pacific and SST being warmer by about 1°C in the rest of the Arctic Ocean (Figure 2c). Lastly, CO_2 concentrations differ between the three control simulations CTR0k, PI, and PLIO as specified in Table 1.

The three control runs are 100 years long, with the first 30 years considered as spin-up. The two Pliocene sensitivity experiments have been branched from the Pliocene control simulation at year 50 and then integrated for further 50 years. The last 30 years of each experiment are considered for the analysis.

3. Results

3.1. Pliocene Control Run

3.1.1. Pliocene Global Climate

Compared to preindustrial (PI), our simulated Pliocene climate (PLIO) is globally warmer during both winter and summer (Figures 3a and 3b). Extratropics exhibit an increase of about 3°C compared to PI in both

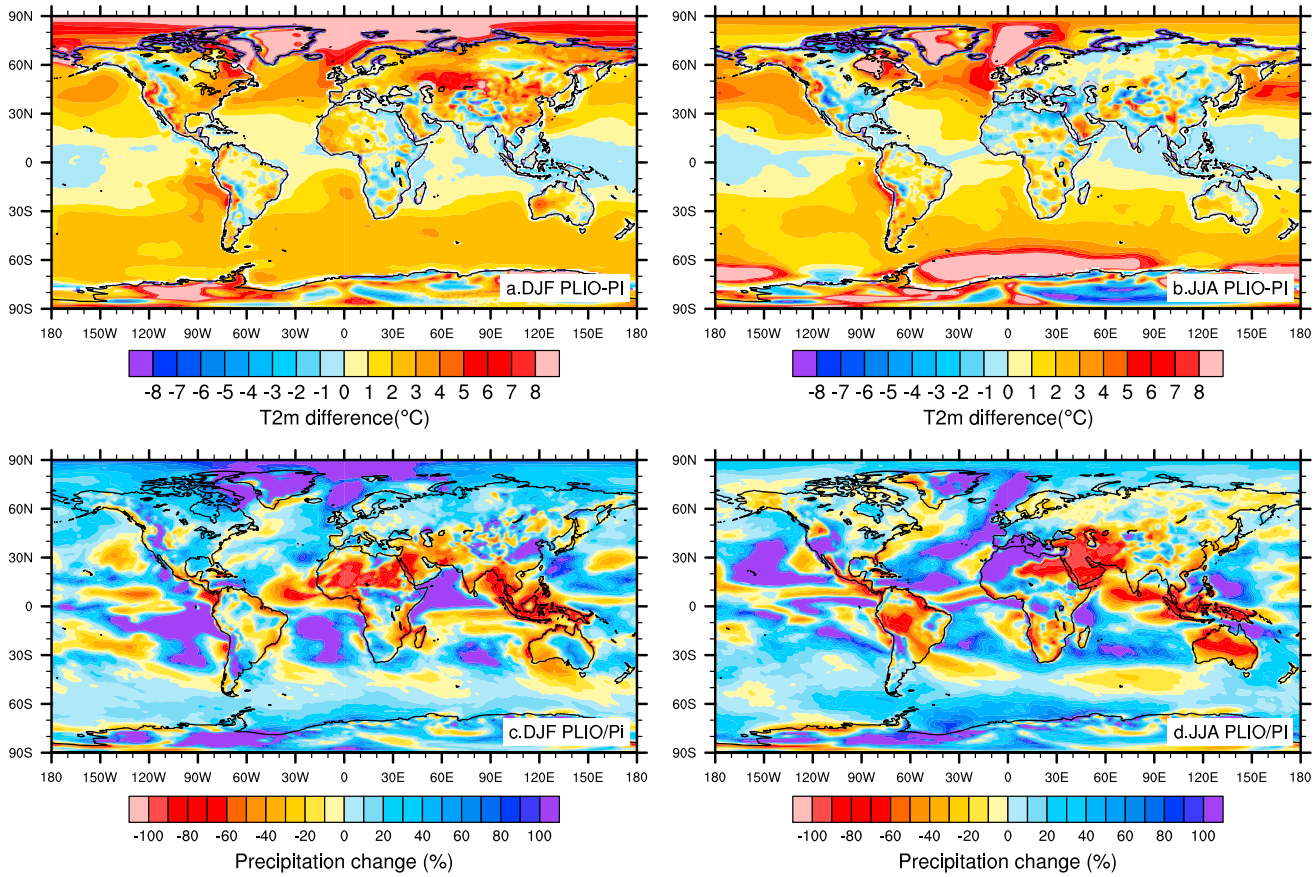

Figure 3. Comparison between preindustrial control run PI and Pliocene control run PLIO. (a) Boreal winter (DJF, December-January-February) surface air temperature difference (°C); (b) boreal summer (JJA, June-July-August) surface air temperature difference (°C); (c) boreal winter precipitation change (in %, PLIO/PI); (d) boreal summer precipitation change (in %, PLIO/PI).

hemispheres. Due to the absence of perennial sea ice cover in the Arctic Ocean and in the Southern Ocean, air temperature increases by about 10°C over the northern high latitudes during boreal winter and over the southern high latitudes during boreal summer (Figures 3a and 3b). Note that the Eastern Equatorial Pacific winter and summer temperatures are higher than preindustrial ones by about 3°C, as expected from the prescribed SST (Figures 3a and 3b). Except in this area, Pliocene tropical and equatorial air temperatures do not significantly differ from preindustrial ones, as a result of PLIO- and PI-prescribed SST, showing no difference over the tropics (Figure 2c). Those simulated regional temperature changes fall in the range of what the geological evidence suggest and are in line with the results of the model simulations from the PlioMIP project [*Haywood et al.*, 2013].

The Pliocene SST presents meridional and zonal gradients that are weaker than preindustrial SST. Those SST patterns may induce substantial changes in the atmospheric synoptic circulation compared to modern circulation. In particular, as reported in previous modeling studies [e.g., *Brierley et al.*, 2009; *Barreiro et al.*, 2006], the absence of a zonal equatorial gradient leads to the weakening of the Walker circulation (Figures 4c and 4d) and the weak meridional SST gradient leads to a weakening of the Hadley circulation (Figures 4e and 4f). Consequently, the convection in the Intertropical Convergence Zone (ITCZ) in the PLIO experiment shrinks (Figure 4a), and due to warmer extratropical SST, the moisture is redistributed north of 30°N and south of 10°S compared to PI (Figure 4b). In the northern high latitudes, the Pliocene winter storm activity weakens compared to preindustrial (Figures 4g and 4h). As a consequence of a lower and smaller Greenland ice sheet in PLIO, the center of storm activity is shifted westward compared to PI. The small Pliocene Greenland ice cap generates a cyclonic circulation over its western part, as shown by 500 hPa winter winds and an anticyclonic circulation over its eastern part (Figure 4h). In addition, because of warmer winter SST and the absence of sea ice in the Nordic Seas, the storm track extends northward.

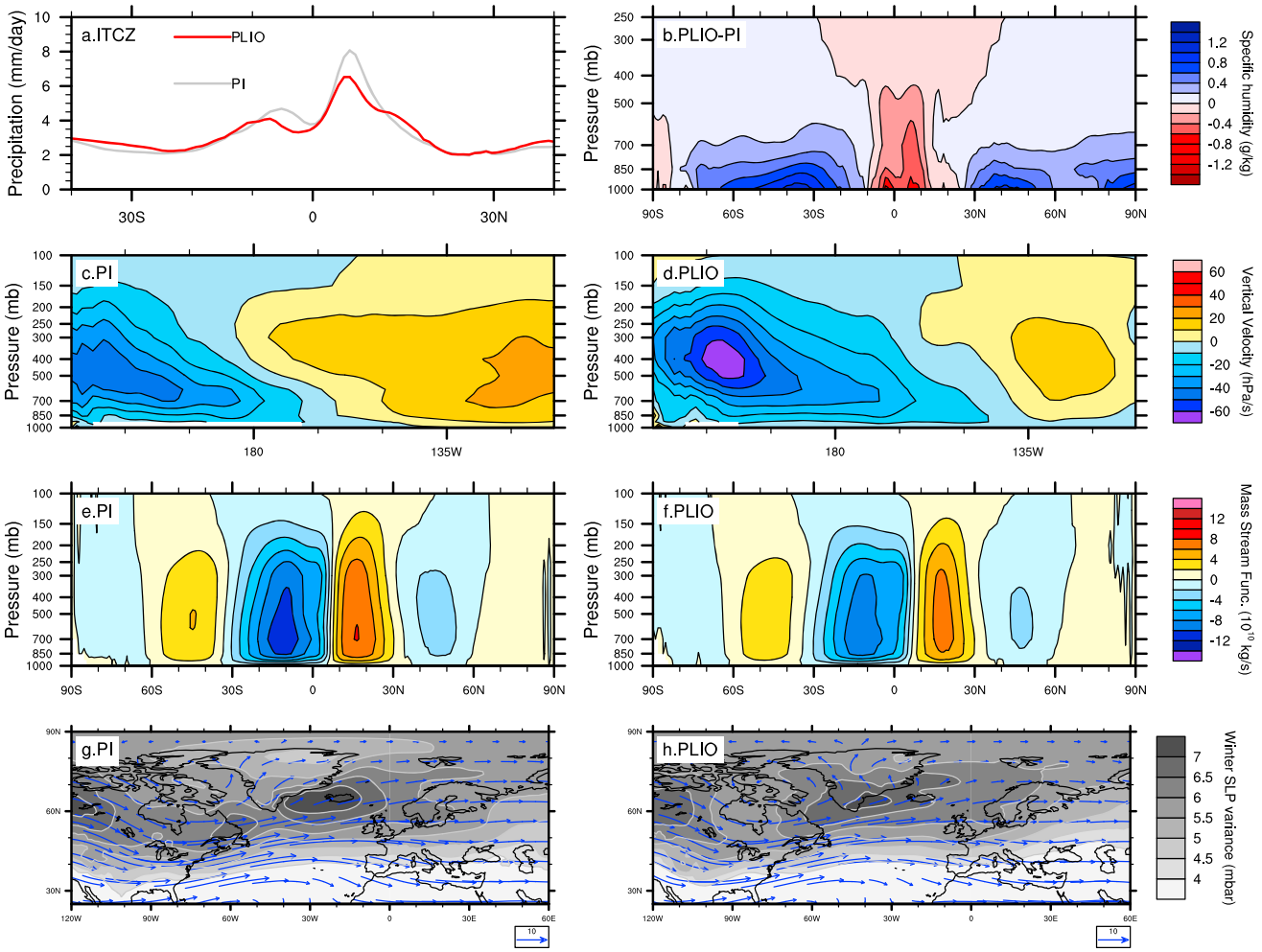

Figure 4. Comparison between preindustrial control run (PI) and Pliocene control run (PLIO). (a) Mean annual zonal precipitation (mm/day); (b) difference in specific humidity (g/kg) between PLIO and PI; (c) Preindustrial Equatorial Pacific (averaged over 5°S–5°N) mean annual atmospheric vertical velocity (hPa/s); (d) same as Figure 4c but for the Pliocene control run; (e) PI global meridional mean annual atmospheric mass stream function (10^{10} kg/s); (f) same as Figure 4e but for the Pliocene control run; (g) preindustrial storm track activity. Storm track activity is represented by the Northern Hemisphere variance of band-pass-filtered (3:7) winter (DJF) sea level pressure (mb), following the method of *Kageyama et al.* [1999]. Arrows correspond to mean annual 500 hPa winds (m/s); (h) Same as Figure 4g but for the Pliocene control run.

Due to the substantial reduction of the sea ice cover over the Arctic Ocean in PLIO, precipitation doubles in the North Atlantic high latitudes compared to PI (Figures 3c and 3d). Similarly, precipitation also increases by about 30% in the Southern Ocean high latitudes as a consequence of less extended sea ice cover. In agreement with the larger specific humidity over midlatitudes, North Atlantic precipitation increases by about 30% during both winter and summer (Figures 3c and 3d). In the tropics, the response of precipitation is complex. Over the upwelling areas, precipitation is doubled compared to preindustrial, while over the equatorial band precipitation decreases by about 40%. In the monsoon areas, precipitation is reduced by more than 60% compared to PI (Figures 3c and 3d), which is consistent with a weakening of both Hadley and Walker circulations.

3.1.2. Pliocene Mediterranean Precipitation Regime

Over the Mediterranean area, Pliocene specific humidity is larger compared to preindustrial (mean latitude 37°N, Figure 4b) and induces precipitation rates higher by about 40% during winter and doubled during summer (Figures 5a and 5b). In fact, in the Pliocene simulation, mean annual evaporation over the sea amounts to 1575 mm/yr against 1372 mm/yr for preindustrial because Pliocene Mediterranean SSTs are warmer (Figures 5c and 5d). Over the Mediterranean borderlands, winter precipitation decreases by about 20% compared to preindustrial (Figure 5a). Conversely, summer precipitation increases by 40% over the

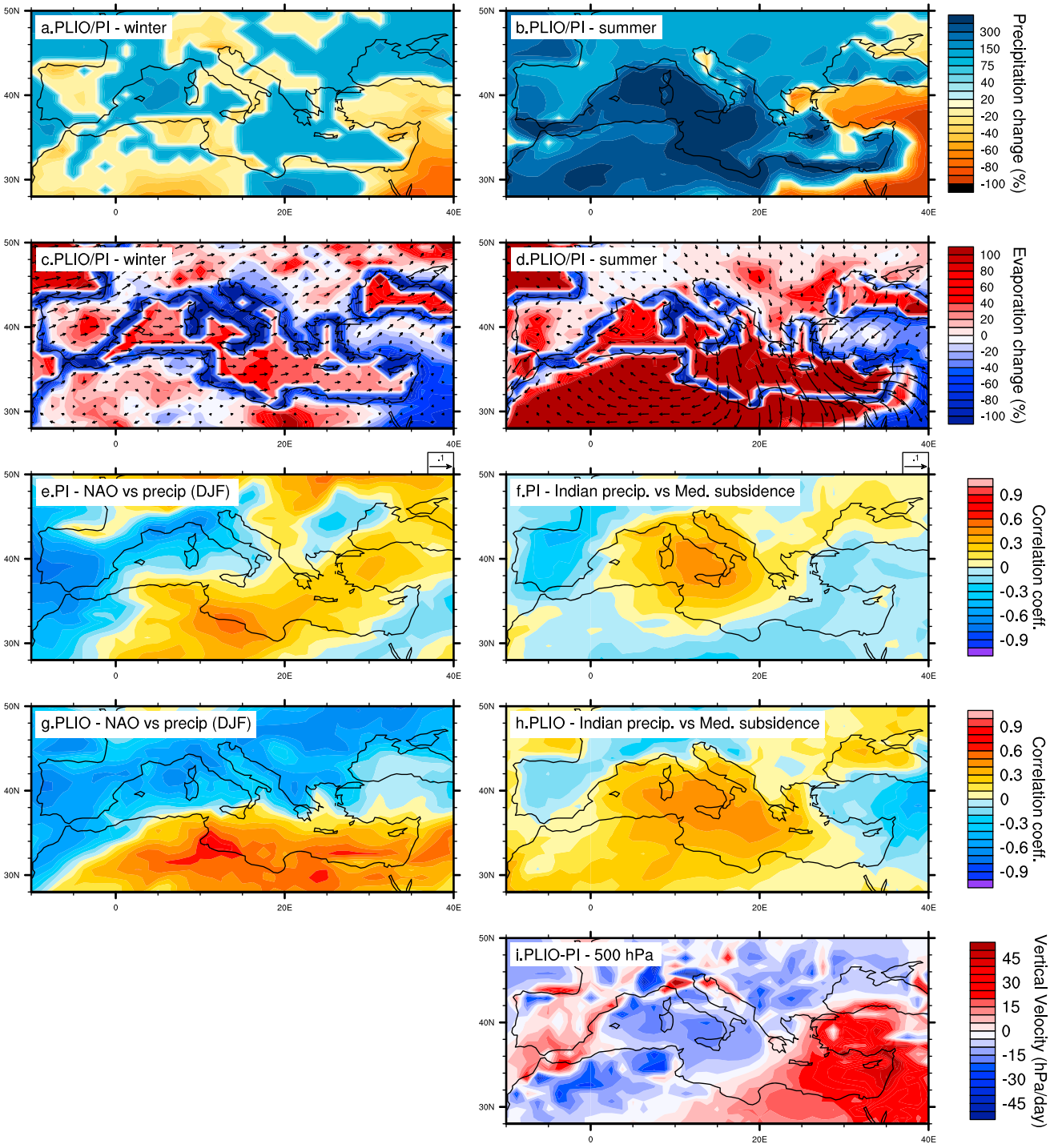

Figure 5. Comparison between PLIO and PI precipitation and main teleconnections over the Mediterranean area. (a) Winter precipitation changes between PLIO and PI (in %); (b) same as Figure 5a but for summer. Note that the color scale is saturated. Precipitation is about 3 times larger over North Africa and up to 10 times larger over the sea in PLIO than in PI; (c) winter evaporation changes between PLIO and PI (in %). Arrows correspond to PLIO winter surface moisture fluxes (m/s); (d) same as Figure 5c but for summer. Note that the color scale is saturated. Evaporation is about 3 times larger in Eastern Mediterranean and 2 times larger over the rest of the Mediterranean; (e) correlation coefficient between NAO and precipitation during winter (DJF) for preindustrial (PI); (f) Correlation coefficient between Indian monsoon precipitation (averaged over 5°N–20°N and 60°E–90°E) and vertical velocity over the Mediterranean during summer (JJA) for preindustrial (PI); (g) same as Figure 5c but for Pliocene (PLIO); (h) same as Figure 5d but for Pliocene (PLIO); (i) difference in summer vertical velocity at 500 hPa between PLIO and PI (hPa/day). The correlations have been computed at 0.95 level.

northern Mediterranean borderlands and is about 4 times larger over North Africa. Over Turkey and the Arabic Peninsula, precipitation decreases by about 40% to 70% during winter and summer, respectively.

In terms of teleconnections, winter precipitation in PLIO is strongly correlated to the winter North Atlantic Oscillation (NAO, Figure 5g). Following *Hurrell et al.* [2003], we computed the winter (December-January-February) Sea Level Pressure Empirical Orthogonal Function (SLP EOF). The NAO corresponds to the leading mode of the SLP EOF, and its positive phase is characterized by a dipole which has a positive maximum located over the Azores area and extends over the entire width of the North Atlantic and a negative maximum located between Iceland and southern Greenland. The percentage of variance explained by the NAO is about 35.8% for present-day CTR0k (36.7% in *Hurrell et al.* [2003], over the period 1899–2001), 41.9% for preindustrial (PI), and 42.7% for Pliocene (PLIO). Correlation between winter precipitation and winter NAO in PLIO is about 0.5 over the Eastern South Mediterranean area and about −0.5 over the Western North Mediterranean area (Figure 5g). This correlation is comparable to that which *Mariotti et al.* [2002] found using present-day reanalysis over the Mediterranean region. In PLIO the correlation is even stronger than in PI and the pattern is more zonal than in PI (Figures 5e and 5g). Despite this strong correlation between the NAO and the precipitation during winter in PLIO, the amount of precipitation induced by the NAO represents only 20% of the total precipitation over the Mediterranean (not shown). Those results suggest that the NAO is a teleconnection that was already well established during the Pliocene, as also shown by *Hill et al.* [2011], and that already influenced the Euro-Mediterranean winter climate about 3 Ma. The NAO is responsible for the PLIO winter precipitation variability over the Mediterranean area. The increase in the amount of precipitation is mostly ruled by the local evaporation of the Mediterranean itself, that is, about 50% times larger than that in PI (Figures 5c and 5d). During summer, the present Eastern Mediterranean is affected by an area of subsidence, whose strength is known to have a connection with the Indian monsoon through the so-called "monsoon-desert" mechanism [*Rodwell and Hoskins*, 1996]. In part, westward propagating Rossby waves excited by the summer Indian monsoon rainfall interact with midlatitude westerlies, enhancing the descending motion mostly in the Eastern Mediterranean [*Tyrlis et al.*, 2013; *Cherchi et al.*, 2014], which contributes to the aridity of the area. To estimate how this mechanism could influence our simulated Mediterranean Pliocene summer precipitation, we calculated the correlation between the summer Indian precipitation, averaged over 5°N–20°N and 60°E–90°E, and the summer vertical velocity at 500 hPa [*Tyrlis et al.*, 2013; *Cherchi et al.*, 2014]. Modern vertical velocity pattern over the Mediterranean area is characterized by a tripole pattern: a subsidence located over the Eastern Mediterranean, uplift over the central Mediterranean, and a subsidence located over Spain. This correlation is simulated both in PI and PLIO (Figures 5f and 5h). In our PI experiment, the positive correlation between monsoon precipitation and midlatitude tropospheric vertical velocity reaches 0.4 in the central part of the Mediterranean (Figure 5f). In PLIO the positive correlation extends to part of the Eastern Mediterranean (Figure 5f). As for the winter NAO, the "monsoon-desert" mechanism affects the distribution of the precipitation during summer over the Mediterranean area.

Changes in the mean climate state are also driven by a similar "monsoon-desert" mechanism that drives the teleconnected interannual variability. In PLIO, the seasonality is lower than in PI, which can lead to a decrease in the monsoon intensity [e.g., *Zhang et al.*, 2013], associated with larger precipitation mostly located in the central part of the Mediterranean (Figure 5b). Higher subsidence over the Eastern Mediterranean, stronger in PLIO than in PI (Figure 5i), agrees with the strong decrease in precipitation simulated over the Eastern Mediterranean borderlands (Figure 5b). Lastly, the amount of precipitation over the Mediterranean area in PLIO results mostly from the local evaporation of the sea, about 3 times larger than in PI (Figure 5d).

3.1.3. Pliocene Mediterranean Runoff

Mediterranean river discharge mirrors the difference in precipitation distribution described in the previous section between Pliocene and modern climate over the borderlands (Figure 6). For convenience, we compare the simulated mean annual river discharge in PLIO with that of the simulated present-day control simulation (CTR0k), which is itself compared to present-day observations from literature. Values for the preindustrial simulation are also reported in Table 2. Note that PI values only slightly differ from that in CTR0k. In order to validate the model performance in terms of river discharge over the Mediterranean area, we compared our present-day simulated runoff to observations taken from various bibliographical sources (Table 2). Values are comparable, even though our simulated present-day river discharge tends to underestimate the range of observations. In CTR0k, as in all our simulations, the Nile river is not dammed and, consequently, the simulated Nile discharge is 1 order of magnitude larger than that in the observations (26,503 m^3/s against observed 1400 m^3/s). When accounting for the observed Nile value instead of the simulated value, the total runoff in the

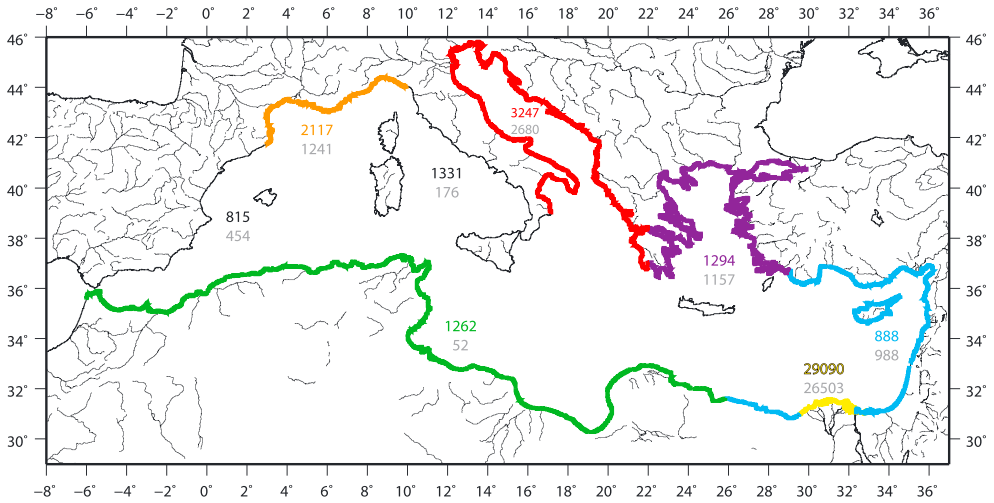

Figure 6. Mean annual runoff discharge (m^3/s) in the various areas of the Mediterranean considered for analysis computed for the Pliocene control run PLIO. Associated numbers in grey correspond to the present-day control run CTR0k values. The Mediterranean coastlines have been divided into seven distinct regions: red corresponds to the Adriatic region, purple corresponds to the Aegean Sea region, blue stands for the Levantine area, yellow is the Nile delta, green includes all the North African rivers, orange includes the Southern France rivers, and the black coastlines correspond to the Iberian rivers and the Tyrrhenian rivers.

Mediterranean amounts to 8148 m^3/s, which is in good agreement with the observed total runoff (8100 m^3/s, Table 2). In spite of the use of an intermediate horizontal resolution of ≈1°, the model is able to simulate a realistic regional distribution of river discharge compared to present-day observations.

Compared with CTR0k, simulated mean annual runoff from the northern Euro-Mediterranean borderland (Iberian coastlines, Gulf of Lion, Italian Tyrrhenian coast, and Adriatic coasts) in PLIO is 2 times larger (Figure 6 and Table 2). The mean annual runoffs into both the Aegean Sea and Levantine basin are comparable in both simulations. The Nile river discharge has been considered separately since it represents 70% of PLIO total Mediterranean river discharge and 78% of CTR0k total river discharge and is consequently 1 order of magnitude larger than all the other mean annual river discharge (Table 2). A remarkable result is the large North African river discharge simulated in our Pliocene control simulation. While in CTR0k the runoff from this area is almost zero, in PLIO this runoff is approaching 1300 m^3/s, which is comparable to the river discharge into the

Table 2. Observed Simulated Mean Annual River Discharge (m^3/s) for the Various Areas of the Mediterranean Displayed in Figure 6[a]

ID	Total	Nile	NA	Adriatic	G. Lion	Levantine	Ag. Sea	Iber	Tyrr.
Observed	8,100[b]	1,400[b]	90[d]	2500[b]	1700[b]	1550–792[c]	2190–1490[c]	995[c]	539[c]
CTR0k	33,893	26,503	52	2680	1241	988	1157	454	176
CTR0k[e]	8,148	1,400	52	2680	1241	988	1157	454	176
PI	29,095	21,312	41	2900	1262	1072	1192	467	198
PLIO	40,997	29,090	1262	3247	2117	888	1294	815	1331
PLIO_EEP	40,320	28,276	1170	3205	2103	1019	1395	1374	796
PLIO_SHNH	30,377	20,508	652	2765	2003	716	1739	470	891

[a]Nile, Nile river; NA, North Africa (without the Nile); Adriatic, Adriatic Sea; G. Lion, Gulf of Lion; Levantine, Levantine basin; Ag. Sea, Agean Sea; Iber, Iberian coasts, and Tyrr., Tyrrhenian Sea.

[b]Observed estimates for present-day Mediterranean river discharge are reported from *Struglia et al.* [2004].

[c]Observed estimates for present-day Mediterranean river discharge are reported from the compilation of *Ludwig et al.* [2009].

[d]Observed estimates for present-day Mediterranean river discharge are reported from the SAGE database (http://www.sage.wisc.edu/riverdata).

[e]In our experiments, the Nile is not dammed. For the comparison, CTR0k corresponds to the present-day river discharge accounting for observed present-day dammed Nile value instead of our simulated value.

Aegean Sea (Table 2). The mean annual river discharge from North Africa is dominated by summer precipitation in the PLIO simulation (Figures 5a and 5b). This large increase in precipitation over North Africa compared to PI is explained by a reduction of the subsidence over this area during summer (Figure 5i). Similarly, the larger Pliocene runoff in the northern Euro-Mediterranean borderland results from a decrease in subsidence over this area during summer. Conversely, in PLIO, the lower runoff simulated in the Levantine basin results from a larger summer subsidence over this area (Figure 5i) and therefore from a decrease in precipitation. Although precipitation decreases largely during both winter and summer over the Levantine borderlands, the larger evaporation occurring over the Eastern Mediterranean leads to a larger eastward moisture advection from the sea to the land regions (Figure 5d).

In conclusion, we show that the spatial distribution of the runoff results primarily from the changes in precipitation distribution over the Euro-Mediterranean area, in turn related to the NAO during winter and the "monsoon-desert mechanism" during summer. While runoff distribution might be influenced by those two teleconnections, the amount of mean annual runoff is dominated by summer precipitation. In PLIO, most of the moisture flux is coming from the evaporation of the Mediterranean Sea itself, which is advected and precipitated over the Southern Mediterranean borderlands (Figure 5d). Furthermore, in the Eastern Mediterranean, the advection of moisture compensates for the increase in subsidence over the Levantine basin, thus contributing to larger precipitation rates over the area (Figures 5d and 5h).

3.2. Plio-Pleistocene Transition

3.2.1. Impact of Global Meridional SST Gradient on the Mediterranean Runoff

When introducing stronger meridional SST gradients, i.e., SST cooling at high and middle latitudes as in PLIO_SHNH experiments, surface air temperature decreases by about 3°C over the Euro-Mediterranean area during both winter and summer. Consequently, atmospheric circulation strengthens during both winter and summer, as illustrated by the mass stream function (Figures 7e and 7f). The winter storm activity also intensifies in the North Atlantic compared to PLIO (Figure 7a). The main center of activity shifts slightly southward and expands from Iceland to the Labrador Sea, which covers a larger area than in the preindustrial simulation (Figure 4g). This can be explained by the effect of Greenland orography, which has a smaller ice cap in PLIO_SHNH than in PI and by a more extensive sea ice cover developing in PLIO_SHNH, in response to the cooler SST forcing. Due to the extratropical and high-latitude cooling, specific humidity north of 20°N and south of 20°S decreases compared to the Pliocene control run (not shown). Consequently, precipitation decreases by about 30% over the Northern Mediterranean borderlands and over North Africa and increases by about 20% over Eastern North Africa during winter compared to PLIO (Figure 7c). The pattern of this precipitation change is a teleconnected response to changes in the North Atlantic storm track (Figure 7a). Correlation between the NAO (not shown) and winter precipitation shows a similar pattern and amplitude than in PI (Figure 5c). Note that in PLIO_SHNH, Mediterranean SST corresponds to that of preindustrial (Figure 2d) and it is cooler than the Pliocene SST by about 3°C on average. This largely reduces the evaporation and therefore decreases the precipitation during both winter and summer over the sea (Figures 7c and 7d).

During summer, the northward shift of ITCZ over Africa is less important in PLIO_SHNH than in PLIO. Consequently, precipitation decreases over the entire North African region by about 50% (Figure 7d). This process is further enhanced by the cooler SSTs, which decrease the amount of moisture advected over the entire Euro-Mediterranean area. Compared to PLIO, the correlation between the Indian monsoon precipitation and this region shows similar patterns but is larger over the central Mediterranean area (up to 0.5, not shown). Because prescribed SSTs are cooler than in PLIO, evaporation decreases in PLIO_SHNH. This leads to lower precipitation over the Levantine basin by about 30%, which is further enhanced by an increase in local subsidence (Figure 7b). Precipitation increases over Turkey by about 30% (Figure 7d), due to the intensification of the cyclonic activity in the Eastern Mediterranean in PLIO_SHNH (about 35 mbar, not shown). In modern conditions, this has been related to the weakening of the Siberian and Azores high [*Krichak et al.*, 2000]. This income of moisture compensates for the large subsidence occurring over this area (Figures 7b and 7d).

As a consequence of the overall precipitation decrease in the Euro-Mediterranean area, the total mean annual runoff generally decreases by 26% compared to PLIO (Table 2). This large reduction is mostly explained by a more moderate Nile discharge (i.e., 20,508 m^3/s against 29,090 in PLIO, Table 2). For all the other areas considered in Figure 6, mean annual runoff is lower than in PLIO (Table 2) and almost reaches preindustrial levels (Table 2). This implies that the mean annual preindustrial Mediterranean runoff results primarily from the strengthening of the meridional SST gradient over the last 3 Ma, causing a southward shift of the ITCZ over

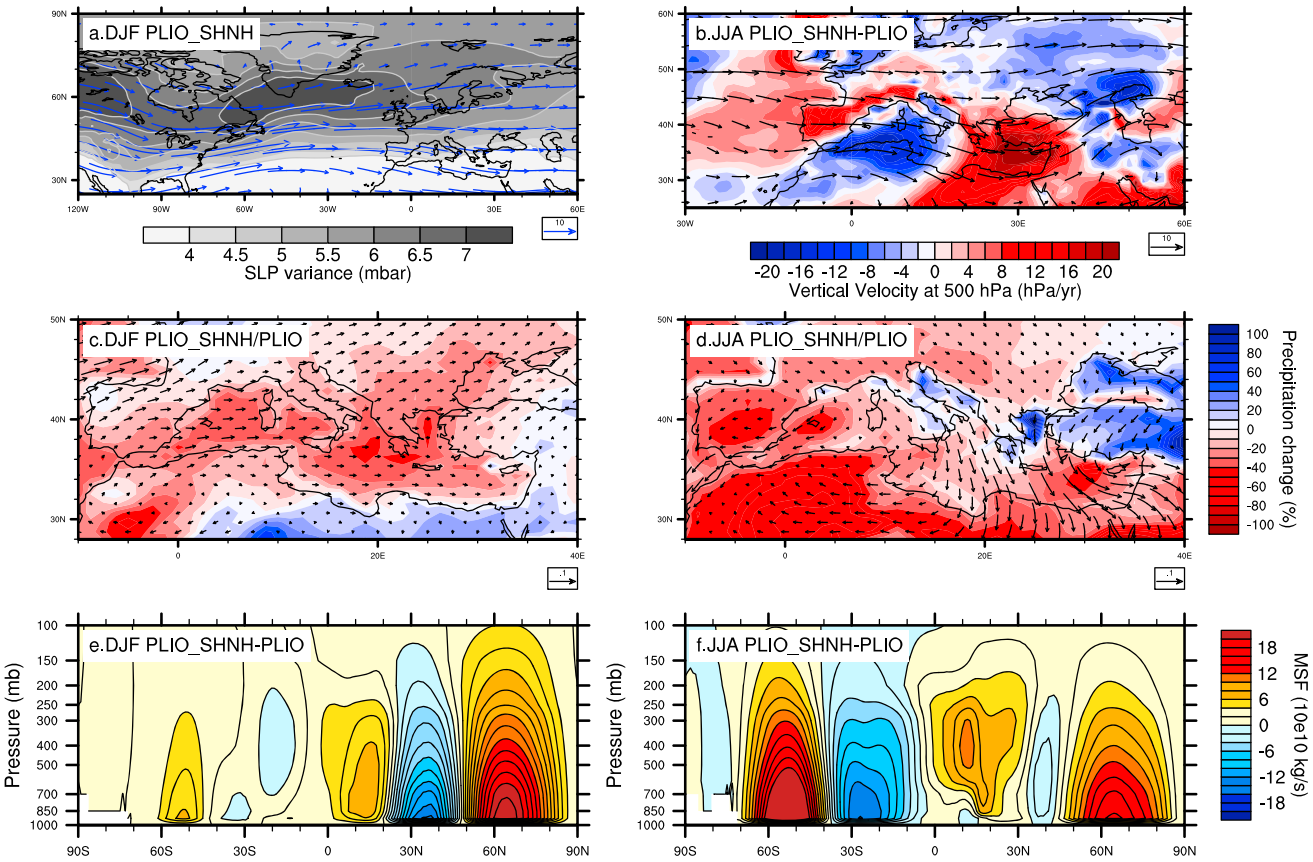

Figure 7. Comparison between PLIO_SHNH and PLIO: (a) Winter (DJF) storm track activity for PLIO_SHNH. Storm track is computed as in Figure 4. Arrows correspond to PLIO_SHNH winter 500 hPa winds (m/s); (b) difference in summer (JJA) vertical velocity at 500 hPa between PLIO_SHNH and PLIO (hPa/yr). Arrows correspond to PLIO_SHNH summer 500 hPa winds (m/s); (c) Winter PLIO_SHNH precipitation change relative to PLIO (in %). Arrows correspond to PLIO_SHNH surface moisture fluxes (m/s); (d) same as Figure 7c but for summer; (e) winter atmospheric mass stream function difference between PLIO_SHNH and PLIO (10^{10} kg/s) averaged over the longitudinal band 17°W–40°E. Note that in this case, the stream function does not conserve the mass (zonal variability is not taken into account) and is plotted to illustrate the changes in atmospheric circulation; (f) same as Figure 7e but for summer. A Student's *t* test at 99% significant level (not shown) reveals that most of the differences between PLIO_SHNH and PLIO are significant, except over Southern France and the Adriatic Sea during summer.

North Africa. Compared to CTR0k, the mean annual runoff in PLIO_SHNH is systematically larger, except in the Levantine area and in the Aegean Sea. The larger amount of runoff in PLIO_SHNH results from a compensation between the strong cooling of air surface temperature causing a drying of the midlatitude climate in PLIO_SHNH and the specific humidity that remains larger than in CTR0k (not shown). In the Levantine area, runoff is less important than in CTR0k because of a stronger subsidence occurring over this area (Figure 2b).

3.2.2. Impact of Global Zonal SST Gradient on the Mediterranean Runoff

As a result of a stronger zonal SST gradient in the tropical band as in the PLIO_EEP experiment, the Walker circulation expands westward compared to PLIO (Figures 8b and 4d). Mean annual temperature decreases over the tropical bands by about 3°C and does not show any other significant temperature changes over the middle and high latitudes (Figure 2e). In response to the colder tropical SST, the atmospheric circulation over the Atlantic weakens during winter but strengthens over the northern midlatitudes and weakens again in the Northern high latitudes (Figure 8e), also inducing a weaker North Atlantic storm activity compared to PLIO (Figure 8a). This alternated circulation pattern has been previously investigated and attributed to Rossby waves, which are found to be excited when an equatorial oceanic cooling occurs and propagate poleward in both hemispheres [*Haarsma and Hazeleger*, 2007]. As a consequence of Rossby waves propagation, in PLIO_EEP, the Northern Hemisphere subtropical jet intensifies, bringing more precipitation over Africa and over the Mediterranean during winter (Figure 8c) and partly compensating for the decrease in winter specific humidity which results from the impact of the stronger zonal SST gradient. The winter NAO explains 42.2% of SLP variance (identical to PLIO). The correlation between winter precipitation and NAO (not shown) exhibits

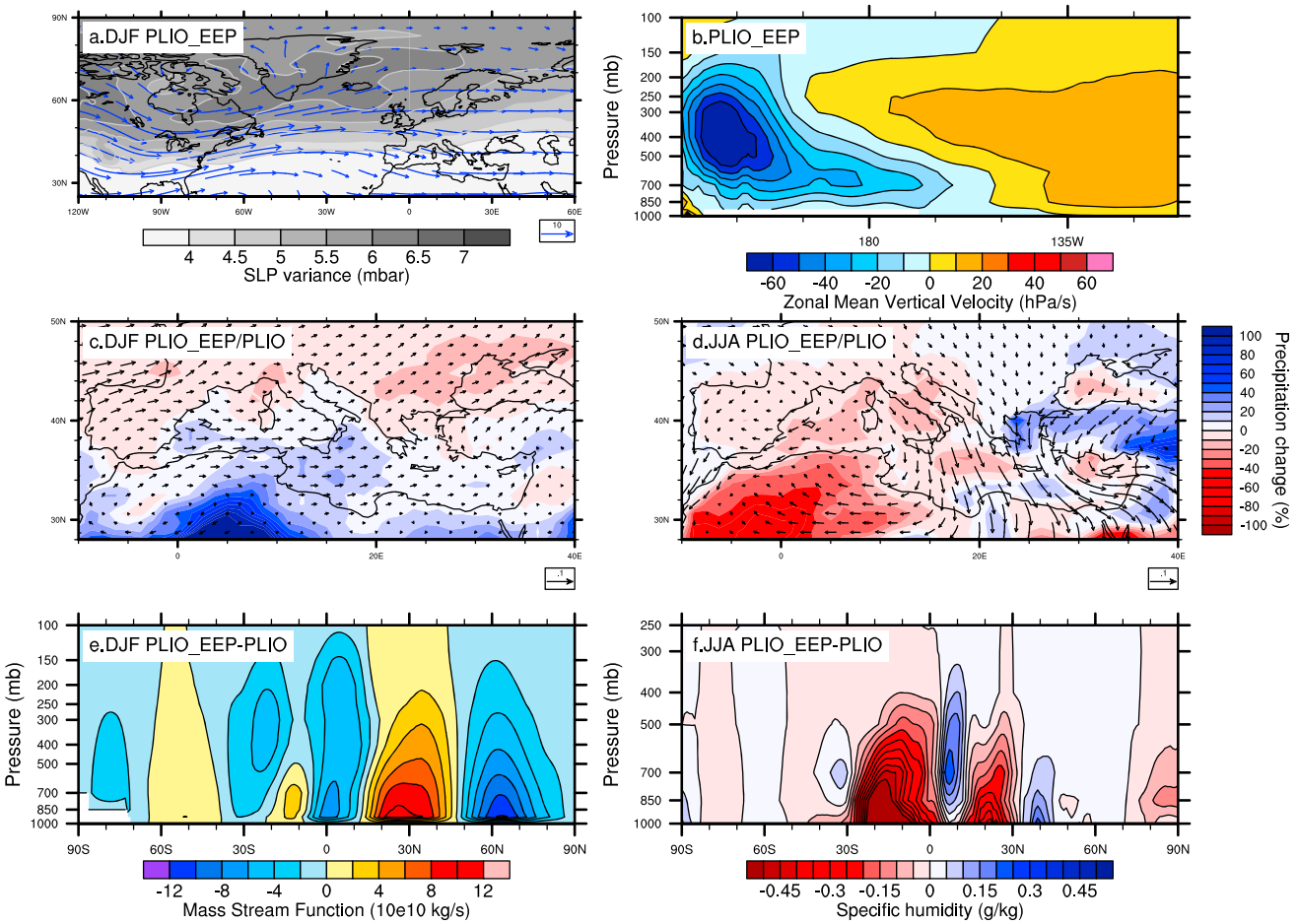

Figure 8. Comparison between PLIO_EEP and PLIO: (a) Winter (DJF) storm track activity for PLIO_EEP. Storm track is computed as in Figure 4. Arrows correspond to PLIO_EEP winter winds at 500 hPa (m/s); (b) mean annual zonal vertical velocity at 500 hPa for PLIO_EEP over the equatorial Pacific, averaged between 5°S and 5°N; (c) winter PLIO_EEP precipitation change relative to PLIO (in %). Arrows correspond to PLIO_EEP surface moisture fluxes (m/s); (d) same a as Figure 8c but for summer; (e) winter atmospheric mass stream function difference (10^{10} kg/s) between PLIO_EEP and PLIO zonally averaged over 17°W–40°E. Note that in this case, the stream function does not conserve the mass (zonal variability is not taken into account) and is plotted to illustrate the changes in atmospheric circulation; (f) summer specific humidity difference between PLIO_EEP and PLIO, averaged over 30°W–30°E (g/kg). A Student's *t* test at 99% significance level (not shown) shows that most of the differences between PLIO_EEP and PLIO are significant, except over the Eastern Mediterranean sea during winter.

a similar spatial pattern but weakens (Figure 5e). The amount of precipitation induced by the NAO represents about 12% of the total precipitation over the Mediterranean area.

During summer, the cooler tropical SST induce a substantial decrease in specific humidity over the tropical band in both hemispheres (Figure 8f), which leads to a reduction in precipitation of about 30% over North Africa (Figure 8d). The correlation between vertical velocity over the Eastern Mediterranean and the Indian monsoon precipitation is similar to that simulated in PLIO (not shown). As a result, no significant changes in the local subsidence over the Mediterranean area occurs. As the monsoon slightly intensifies in PLIO_EEP compared to PLIO, the decrease in local subsidence occurring between the Caspian and the Black Sea is larger, increasing precipitation by about 15% over the Caspian-Black Sea area (Figure 8d). Due to the convergence of moisture fluxes coming from this area, precipitation also increases by about 20% over the Aegean Sea and by about 15% over the Levantine borderlands (Figure 8d).

Overall, a stronger zonal SST gradient with respect to PLIO does not have an impact as large as meridional gradient on our simulated Euro-Mediterranean climate. In fact, the mean annual total runoff in PLIO_EEP is similar to that of PLIO (Table 2). In terms of runoff, the only noticeable differences occur over North Africa, where PLIO_EEP runoff is lower than PLIO by about 100 m^3/s and over the Levantine area and in the Aegean Sea, where runoff is larger than PLIO by about 100 m^3/s (Table 2). However, the causes of discrepancies for those regions differ. For North Africa, the increase in mean annual runoff is caused by an increase in winter

Table 3. Simulated Mean Annual Mediterranean Hydrological Cycle (mm/yr)[a]

ID	Total ($E - P - R$)	Evaporation	Precipitation	Runoff
Observed	321–1130	1570–934	310–700	100
Mariotti et al.	503–580	934–1113	331–504	100
CTR0k[b]	934	1381	336	111
PI	655	1372	360	357
PLIO	538	1575	528	509
PLIO_EEP	535	1578	543	500
PLIO_SHNH	744	1476	368	364

[a]In the calculations, the Mediterranean area equals 2.5×10^{12} km^2.
[b]CTR0k accounts for the observed dammed Nile river discharge from *Mariotti et al.* [2002] instead of our simulated Nile discharge. Observation of the various components of the Mediterranean hydrological cycle are from *Mariotti et al.* [2002], and references there in.

precipitation. The net effect of the zonal SST gradient over North Africa on annual basis is to decrease precipitation, thus reducing the amount of runoff occurring in PLIO_EEP with respect to PLIO. The increase in mean annual runoff for the Levantine borderlands and the Aegean Sea, on the contrary, results from larger summer precipitation (Figures 8c and 8d).

3.2.3. Mediterranean Hydrological Cycle Across the Plio-Pleistocene Transition

Our simulations show that during the Pliocene, the river discharge into the Mediterranean was 40% larger than during preindustrial period and about 20% larger than during present day (considering the simulated Nile discharge values, i.e., without dam, Table 2). One of the main features of the Pliocene Mediterranean runoff is the active Northwest African rivers network, inducing a discharge 30 times larger than under modern climate conditions in our simulations. On the other hand, the river discharge in the Levantine basin was slightly reduced during the Pliocene. In the previous sections we show that when the meridional SST gradient strengthens (PLIO_SHNH), total runoff is almost reduced to its preindustrial value and North African runoff is 2 times smaller than in our Pliocene control run. This is a direct consequence of the southward shift of the ITCZ over Africa and of the reduction of evaporation over the Mediterranean Sea. On the contrary, we show that when departing from our Pliocene control run, the main influence of a stronger zonal equatorial SST gradient is to increase the river discharge from the Eastern Mediterranean borderlands. What are the consequences of the Pliocene Mediterranean climate and river discharge on the Mediterranean hydrological budget?

The surface hydrological cycle is calculated as $E - P - R$ where E is the mean annual evaporation over the Mediterranean Sea, P is the total mean annual precipitation over the Mediterranean Sea and R is the mean annual river discharge into the Mediterranean. Simulated present-day hydrological budget in CTR0k, accounting for dammed Nile river discharge, has a freshwater deficit of about 934 mm/yr (Table 3). The value is in the range of what observations suggest (Table 3). However, using several reanalysis, *Mariotti et al.* [2002] found a deficit of about 500 mm/yr. The discrepancy between our CTR0k simulated hydrological cycle and the estimate by *Mariotti et al.* [2002] comes from an excessive simulated evaporation over the sea, as shown in Table 3. This might be due to the fact that we performed climate simulations with forced SST and, therefore, the interaction between atmosphere and ocean is not accounted for. Mean annual precipitation and runoff are, on the contrary, perfectly in line with observations.

In our Pliocene control simulation, the deficit in water over the Mediterranean is lower than in our present-day simulation, due to a larger river discharge (Table 3). Compared to CTR0k, evaporation is larger by about 200 mm/yr but is compensated for by an increase in mean annual precipitation of the same order. It is the larger river discharge, by about 400 mm/yr, which mostly contributes to reduce the water deficit over the Mediterranean from 934 mm/yr to 538 mm/yr. The hydrological budget is identical over the Mediterranean when accounting for a zonal equatorial SST cooling (PLIO_EEP). On the contrary, the deficit in water increases by about 200 mm/yr compared to PLIO when accounting for extratropical SST cooling (PLIO_SHNH). This is due to a reduction of about 150 mm/yr both in precipitation and runoff and a reduction of about 100 mm/yr in mean annual evaporation compared to the Pliocene value. Note that in PLIO_SHNH, mean annual precipitation over the Mediterranean is similar to that of preindustrial and present day implying that

what mainly determines the modern precipitation regime over the Mediterranean is the development of the meridional SST gradient.

4. Conclusion

With this work, we wanted to explore the impact of the strengthening of the global meridional and zonal SST gradients on the Mediterranean runoff variability and precipitation regime across the Plio-Pleistocene transition, that occurred about 3 Ma. In addition to present-day and preindustrial simulations, three Pliocene simulations were carried out, a Pliocene control run, a Pliocene simulation with cooler extratropics SST, and a Pliocene simulation accounting for cooler tropical SST. Based on the analysis of those simulations, we show the following:

1. The warmer extratropical SSTs during the Pliocene period cause the subtropics and high latitudes to experience larger precipitation rates due to an increase in specific humidity. Both Hadley and Walker circulations are weaker than during preindustrial, in agreement with previous modeling studies.
2. The main teleconnections acting upon the Euro-Mediterranean area, i.e., the North Atlantic Oscillation during winter and the "monsoon-desert" mechanism in summer were at work during the Pliocene.
3. In our Pliocene simulation, North Africa's hydrological network is by far more active than today. This can be explained by the larger simulated humidity over this region, resulting from the reduction of zonal and meridional SST gradients. In addition, it implies that the descending branch of the Hadley cell reached higher latitudes during the Pliocene than today. In fact, as soon as we account for a stronger meridional SST gradient, river discharge from this area reduces substantially.
4. In our preindustrial and present-day simulations, the river discharge from the Levantine area is larger than in our Pliocene simulations. This value increases only when introducing the zonal equatorial SST gradient. During summer, the impact of this gradient is to shift the main center of subsidence over the Eastern Mediterranean southward of its Pliocene position. This consequently shifts the geographical limit of summer aridity in this region and allows for more precipitation over the Levantine basin.
5. In our Pliocene simulation, the Mediterranean hydrological budget has a reduced water deficit because of a larger river discharge. The zonal equatorial SST gradient does not have any significant consequences on the Pliocene Mediterranean hydrological cycle. On the contrary, when extratropical SSTs cool, the water deficit increases mainly because of a decrease in precipitation and runoff.

Those conclusions suggest that the modern atmospheric circulation over the Mediterranean area started to develop at least 3 Ma and reached almost present-day configuration in terms of teleconnection strength around 1.8 Ma, when the cold tongues expanded substantially in the Eastern Equatorial Pacific and Atlantic. Finally, our results also suggest that in a mean background climate state significantly warmer than today, the induced changes of the Hadley circulation could potentially lead to an increase in water resources in Northwest Africa.

Acknowledgments
We gratefully acknowledge the support of Italian Ministry of Education and the Programma Nazionale Ricerche in Antartide. The numerical data used in the present contribution have been simulated by F. Colleoni. Data are freely available on request to the corresponding author.

References

Barreiro, M., G. Philander, R. Pacanowski, and A. Fedorov (2006), Simulations of warm tropical conditions with application to middle Pliocene atmospheres, *Clim. Dyn.*, *26*(4), 349–365.

Bertini, A. (2010), Pliocene to Pleistocene palynoflora and vegetation in Italy: State of the art, *Quat. Int.*, *225*(1), 5–24.

Brierley, C. M., and A. V. Fedorov (2010), Relative importance of meridional and zonal sea surface temperature gradients for the onset of the ice ages and Pliocene-Pleistocene climate evolution, *Paleoceanography*, *25*, PA2214, doi:10.1029/2009PA001809.

Brierley, C. M., A. V. Fedorov, Z. Liu, T. D. Herbert, K. T. Lawrence, and J. P. LaRiviere (2009), Greatly expanded tropical warm pool and weakened Hadley circulation in the early Pliocene, *Science*, *323*(5922), 1714–1718.

Cherchi, A., H. Annamalai, S. Masina, and A. Navarra (2014), South Asian summer monsoon and the eastern Mediterranean climate: The monsoon-desert mechanism in CMIP5 simulations, *J. Clim.*, *27*, 6877–6903.

Colleoni, F., S. Masina, A. Negri, and A. Marzocchi (2012), Plio-Pleistocene high-low latitude climate interplay: A Mediterranean point of view, *Earth Planet. Sci. Lett.*, *319-320*, 35–44.

Dolan, A. M., A. M. Haywood, D. J. Hill, H. J. Dowsett, S. J. Hunter, D. J. Lunt, and S. J. Pickering (2011), Sensitivity of Pliocene ice sheets to orbital forcing, *Palaeogeogr. Palaeoclimatol. Palaeoecol.*, *1-2*, 98–110.

Dowsett, H., J. Barron, and R. Z. Poore (1996), Middle Pliocene sea surface temperatures: A global reconstruction, *Mar. Micropaleontol.*, *27*, 13–25.

Dowsett, H., M. Robinson, and K. Foley (2009), Pliocene three-dimensional global ocean temperature reconstruction, *Clim. Past*, *5*(4), 769–783.

Etourneau, J., R. Schneider, T. Blanz, and P. Martinez (2010), Intensification of the Walker and Hadley atmospheric circulations during the Pliocene-Pleistocene climate transition, *Earth Planet. Sci. Lett.*, *297*, 103–110.

Fedorov, A. V., P. S. Dekens, M. McCarthy, A. C. Ravelo, P. B. deMenocal, M. Barreiro, R. C. Pacanowski, and S. G. Philander (2006), The Pliocene paradox (Mechanisms for a permanent El Niño), *Science*, *312*, 1485–1489.

Fedorov, A. V., C. Brierley, K. Lawrence, Z. Liu, P. Dekens, and A. Ravelo (2013), Patterns and mechanisms of early Pliocene warmth, *Nature*, *496*, 43–49.
Giorgi, F. (2006), Climate change hot-spots, *Geophys. Res. Lett.*, *33*, L08707, doi:10.1029/2006GL025734.
Haarsma, R. J., and W. Hazeleger (2007), Extratropical atmospheric response to equatorial Atlantic cold tongue anomalies, *J. Clim.*, *20*(10), 2076–2091.
Haug, G. H., et al. (2005), North Pacific seasonality and the glaciation of North America 2.7 million years ago, *Nature*, *433*(7028), 821–825.
Haywood, A., et al. (2010), Pliocene model intercomparison project (PlioMIP): Experimental design and boundary conditions (experiment 1), *Geosci. Model Dev.*, *3*(1), 227–242.
Haywood, A., et al. (2013), Large-scale features of Pliocene climate: Results from the Pliocene Model Intercomparison Project, *Clim. Past*, *9*, 191–209.
Haywood, A. M., H. J. Dowsett, M. M. Robinson, D. K. Stoll, A. M. Dolan, D. J. Lunt, B. Otto-Bliesner, and M. A. Chandler (2011), Pliocene Model Intercomparison Project (PlioMIP): Experimental design and boundary conditions (experiment 2), *Geosci. Model Dev.*, *4*, 571–577.
Herbert, T. D., G. Ng, and L. C. Peterson (2015), Evolution of Mediterranean sea surface temperatures 3.5–1.5 Ma: Regional and hemispheric influences, *Earth Planet. Sci. Lett.*, *409*, 307–318.
Hill, D., A. Csank, A. Dolan, and D. Lunt (2011), Pliocene climate variability: Northern Annular Mode in models and tree-ring data, *Palaeogeogr. Palaeoclimatol. Palaeoecol.*, *1-2*, 118–127.
Hurrell, J. W., Y. Kushnir, G. Ottersen, and M. Visbeck (2003), An overview of the North Atlantic Oscillation, in *The North Atlantic Oscillation: Climatic Significance and Environmental Impact*, edited by J. W. Hurrell et al., AGU, Washington, D. C.
Jansen, E., T. Fronval, F. Rack, and J. E. Channell (2000), Pliocene-Pleistocene ice rafting history and cyclicity in the Nordic Seas during the last 3.5 Myr, *Paleoceanography*, *15*(6), 709–721.
Kageyama, M., P. J. Valdes, G. Ramstein, C. Hewitt, and U. Wyputta (1999), Northern Hemisphere storm tracks in present day and last glacial maximum climate simulations: A comparison of the European PMIP models, *J. Clim.*, *12*, 742–760.
Krichak, S., M. Tsidulko, and P. Alpert (2000), Monthly synoptic patterns associated with wet/dry conditions in the eastern Mediterranean, *Theor. Appl. Climatol.*, *65*(3–4), 215–229.
Krijgsman, W., F. Hilgen, I. Raffi, F. Sierro, and D. Wilson (1999), Chronology, causes and progression of the Messinian salinity crisis, *Nature*, *400*(6745), 652–655.
Lawrence, K., S. Sosdian, H. White, and Y. Rosenthal (2010), North Atlantic climate evolution through the Plio-Pleistocene climate transitions, *Earth Planet. Sci. Lett.*, *300*, 329–342.
Leroy, S., and L. Dupont (1994), Development of vegetation and continental aridity in northwestern Africa during the Late Pliocene: The pollen record of ODP Site 658, *Palaeogeogr. Palaeoclimatol. Palaeoecol.*, *109*(2–4), 295–316.
Lisiecki, L., and M. Raymo (2005), A pliocene-pleistocene stack of 57 globally distributed benthic δ^{18}O records, *Paleoceanography*, *20*, PA1003, doi:10.1029/2004PA001071.
Lourens, L. (2004), Revised tuning of Ocean Drilling Program Site 964 and KC01B (Mediterranean) and implications for the δ^{18}O, tephra, calcareous nannofossil, and geomagnetic reversal chronologies of the past 1.1 Myr, *Paleoceanography*, *19*, PA3010, doi:10.1029/2003PA000997.
Lourens, L., F. Hilgen, L. Gudjonsson, and W. Zachariasse (1992), Late Pliocene to early Pleistocene astronomically forced sea surface productivity and temperature variations in the Mediterranean, *Mar. Micropaleontol.*, *19*, 49–78.
Ludwig, W., E. Dumont, M. Meybeck, and S. Heussner (2009), River discharges of water and nutrients to the Mediterranean and Black Sea: Major drivers for ecosystem changes during past and future decades?, *Prog. Oceanogr.*, *80*(3), 199–217.
Mariotti, A., M. V. Struglia, N. Zeng, and K. Lau (2002), The hydrological cycle in the Mediterranean region and implications for the water budget of the Mediterranean Sea, *J. Clim.*, *15*(13), 1674–1690.
Martinez-Garcia, A., A. Rosell-Mele, E. L. McClymont, R. Gersonde, and G. H. Haug (2010), Subpolar link to the emergence of the modern equatorial Pacific Cold Tongue, *Science*, *328*, 1550–1553.
McKay, R., et al. (2012), Antarctic and Southern Ocean influences on Late Pliocene global cooling, *Proc. Nat. Acad. Sci.*, *109*(17), 6423–6428.
Neale, R. B., J. Richter, S. Park, P. H. Lauritzen, S. J. Vavrus, P. J. Rasch, and M. Zhang (2013), The mean climate of the Community Atmosphere Model (CAM4) in forced SST and fully coupled experiments, *J. Clim.*, *26*(14), 5150–5168.
Niu, G.-Y., Z.-L. Yang, R. Dickinson, L. Gulden, and H. Su (2007), Development of a simple groundwater model for use in climate models and evaluation with Gravity Recovery and Climate Experiment data, *J. Geophys. Res.*, *112*, D07103, doi:10.1029/2006JD007522.
O'Brien, C., G. Foster, M. Martínez-Botí, R. Abell, J. Rae, and R. Pancost (2014), High sea surface temperatures in tropical warm pools during the Pliocene, *Nat. Geosci.*, *7*(8), 606–611.
Oleson, K., et al. (2008), Improvements to the Community Land Model and their impact on the hydrological cycle, *J. Geophys. Res.*, *113*, G01021, doi:10.1029/2007JG000563.
Pagani, M., Z. Liu, J. LaRiviere, and A. Ravelo (2010), High Earth-system climate sensitivity determined from Pliocene carbon dioxide concentrations, *Nat. Geosci.*, *3*, 27–30.
Polyak, L., et al. (2010), History of sea ice in the Arctic, *Quat. Sci. Rev.*, *29*(15), 1757–1778.
Polyak, L., K. M. Best, K. A. Crawford, E. A. Council, and G. St-Onge (2013), Quaternary history of sea ice in the western Arctic Ocean based on foraminifera, *Quat. Sci. Rev.*, *79*, 145–156.
Raicich, F., N. Pinardi, and A. Navarra (2003), Teleconnections between Indian monsoon and Sahel rainfall and the Mediterranean, *Int. J. Climatol.*, *23*(2), 173–186.
Ravelo, A., H. Dyke, A. Lyle, A. Lyle, and M. Wara (2004), Regional climate shifts caused by gradual global cooling in the Pliocene epoch, *Nature*, *429*, 263–267.
Raymo, M., J. Mitrovica, M. O'Leary, R. DeConto, and P. Hearty (2011), Departures from eustasy in Pliocene sea-level records, *Nat. Geosci.*, *4*(5), 328–332.
Rayner, N., D. E. Parker, E. Horton, C. Folland, L. Alexander, D. Rowell, E. Kent, and A. Kaplan (2003), Global analyses of sea surface temperature, sea ice, and night marine air temperature since the late nineteenth century, *J. Geophys. Res.*, *108*(D14), 4407, doi:10.1029/2002JD002670.
Rodwell, M., and B. Hoskins (1996), Monsoons and the dynamics of deserts, *Q. J. R. Meteorol. Soc.*, *122*(534), 1385–1404.
Rosenbloom, N. A., B. L. Otto-Bliesner, E. C. Brady, and P. J. Lawrence (2013), Simulating the mid-Pliocene warm period with the CCSM4 model, *Geosci. Model Dev.*, *6*, 549–561.
Rossignol-Strick, M. (1985), Mediterranean Quaternary sapropels, an immediate response of the African monsoon to variation of insolation, *Palaeogeogr. Palaeoclimatol. Palaeoecol.*, *49*, 237–263.
Rossignol-Strick, M., W. Nesteroff, P. Olive, and C. Vergnaud-Grazzini (1982), After the deluge: Mediterranean stagnation and sapropel formation, *Nature*, *295*, 105–110.

Roveri, M., et al. (2014), The Messinian salinity crisis: Past and future of a great challenge for marine sciences, *Mar. Geol.*, *352*, 25–58.
Salzmann, U., A. M. Haywood, D. Lunt, P. Valdes, and D. Hill (2008), A new global biome reconstruction and data-model comparison for the middle Pliocene, *Global Ecol. Biogeogr.*, *17*(3), 432–447.
Sohl, L., M. Chandler, R. Schmunk, K. Mankoff, J. Jonas, K. Foley, and H. Dowsett (2009), *PRISM3/GISS Topographic Reconstruction: US Geological Survey Data Series 419*, U.S. Geol. Surv., Reston, Va.
Struglia, M., A. Mariotti, and A. Filograsso (2004), River discharge into the Mediterranean Sea: Climatology and aspects of the observed variability, *J. Clim.*, *17*(24), 4740–4751.
Tyrlis, E., J. Lelieveld, and B. Steil (2013), The summer circulation in the eastern Mediterranean and the Middle East: Influence of the South Asian monsoon and mid-latitude dynamics, in *Advances in Meteorology, Climatology and Atmospheric Physics*, pp. 793–802, Springer, Berlin.
Wang, P., J. Tian, and L. Lourens (2010), Obscuring of long eccentricity cyclicity in Pleistocene oceanic carbon isotope records, *Earth Planet. Sci. Lett.*, *290*, 319–330.
Wara, M. W., A. C. Ravelo, and M. L. Delaney (2005), Permanent El Niño-like conditions during the Pliocene warm period, *Science*, *309*(5735), 758–761.
Zhang, R., et al. (2013), Mid-pliocene east Asian monsoon climate simulated in the PlioMIP, *Clim. Past*, *9*(5), 2085–2099.